Superscattering of a pseudospin-1 wave in a photonic lattice

Hongya Xu[1] and Ying-Cheng Lai[1,2,*]

[1]*School of Electrical, Computer, and Energy Engineering, Arizona State University, Tempe, Arizona 85287, USA*

[2]*Department of Physics, Arizona State University, Tempe, Arizona 85287, USA*

(Received 8 November 2016; revised manuscript received 7 December 2016; published 17 January 2017)

We uncover a superscattering behavior of a pseudospin-1 wave from weak scatterers in the subwavelength regime where the scatterer size is much smaller than the wavelength. The phenomenon manifests itself as unusually strong scattering characterized by extraordinarily large values of the cross section even for arbitrarily weak scatterer strength. We establish analytically and numerically that the physical origin of superscattering is revival resonances, for which the conventional Born theory breaks down. The phenomenon can be experimentally tested using synthetic photonic systems.

DOI: 10.1103/PhysRevA.95.012119

I. INTRODUCTION

In wave scattering, a conventional and well-accepted notion is that weak scatterers lead to weak scattering. This can be understood by resorting to the Born approximation. Consider a simple two-dimensional (2D) setting where particles are scattered from a circular potential of height V_0 and radius R. In the low-energy (long-wavelength) regime $kR < 1$ (with k being the wave vector), the Born approximation holds for weak potential: $(m/\hbar^2)|V_0|R^2 \ll 1$. Likewise, in the high-energy (short-wavelength) regime characterized by $kR > 1$, the Born approximation still holds in the weak-scattering regime: $(m/\hbar^2)|V_0|R^2 \ll (kR)^2$. In general, whether scattering is weak or strong can be quantified by the scattering cross section. For scalar waves governed by the Schrödinger equation, in the Born regime the scattering cross section can be expressed as polynomial functions of the effective potential strength and size [1]. For spinor waves described by the Dirac equation (e.g., graphene systems), the 2D transport cross section is given by [2] $\Sigma_{\rm tr}/R \simeq (\pi^2/4)(V_0R)^2(kR)$ (under $\hbar v_F = 1$). In light scattering from spherically dielectric, "optically soft" scatterers with relative refractive index n near unity, i.e., $kR|n-1| \ll 1$, the Born approximation manifests itself as an exact analog of the Rayleigh-Gans approximation [3], which predicts that the scattering cross section behaves as $\Sigma/(\pi R^2) \sim |n-1|^2(kR)^4$ in the small scatterer size limit $kR \ll 1$. In wave scattering, the conventional understanding is then that a weak scatterer leads to a small cross section and, consequently, to weak scattering, and this holds regardless of the nature of the scattering particle or wave, i.e., vector, scalar, or spinor.

In this paper, we report a counterintuitive phenomenon that defies the conventional wisdom that a weak scatterer always results in weak scattering. The phenomenon occurs in scattering of higher spinor waves, such as pseudospin-1 particles that can arise in experimental synthetic photonic systems whose energy-band structure consists of a pair of Dirac cones and a flat band through the conical intersection point [4–11]. Theoretically, pseudospin-1 waves are effectively described by the generalized Dirac-Weyl equation [7,12–17]: $H_0\Psi = \boldsymbol{S}\cdot\boldsymbol{k}\Psi = E\Psi$, with $\Psi = [\Psi_1,\Psi_2,\Psi_3]^T$, $\boldsymbol{k} = (k_x,k_y)$, and $\boldsymbol{S} = (S_x,S_y)$ being the vector of 3×3 matrices for spin-1 particles. Investigating the general scattering of pseudospin-1 wave, we find the surprising and counterintuitive phenomenon that extraordinarily strong scattering, or superscattering, can emerge from arbitrarily weak scatterers at sufficiently low energies (i.e., in the deep-subwavelength regime). Accompanying this phenomenon is a type of resonance that can persist at low energies for weak scatterers. We provide an analytic understanding of the resonance and derive formulas for the resulting cross section, with excellent agreement with results from direct numerical simulations. We also propose experimental verification schemes using photonic systems.

II. RESULTS

We consider scattering of 2D pseudospin-1 particles from a circularly symmetric scalar potential barrier of height V_0 defined by $V(r) = V_0\Theta(R-r)$, where R is the scatterer radius and Θ denotes the Heaviside function. The band structure of pseudospin-1 particles can be illustrated using a 2D photonic lattice for a transverse electromagnetic wave with the electric field along the z axis. As demonstrated in previous works [4,17], Dirac cones induced by accidental degeneracy can emerge at the center of the Brillouin zone for proper material parameters, about which a three-component structured light wave emerges and is governed by the generalized Dirac-Weyl equation.

We consider the setting of photonic crystal to illustrate the pseudospin-1 band structure. Figure 1(a) shows the band structure of lattices with a triangular configuration constructed by cylindrical alumina rods in air, where the rod radius is $r_0 = 0.203a$ (a is the lattice constant) and the rod dielectric constant is 8.8 [4]. We obtain an accidental-degeneracy-induced Dirac point at the center of the first Brillouin zone at the finite frequency of $0.6357\times 2\pi\times c/r_0$. Following a general lattice-scaling scheme of photonic gate potential [17], we obtain a sketch of the cross section of the lattice in the plane, as shown in Fig. 1(b), where the thick black bar denotes an applied exciter. For our scattering problem, the band structures outside and inside of the scatterer are shown in Fig. 1(c).

The scattering problem can be treated analytically using the Dirac-Weyl equation (see Appendix A for a detailed derivation of the various scattering formulas). To demonstrate the phenomenon of superscattering, we use the transport cross

*Ying-Cheng.Lai@asu.edu

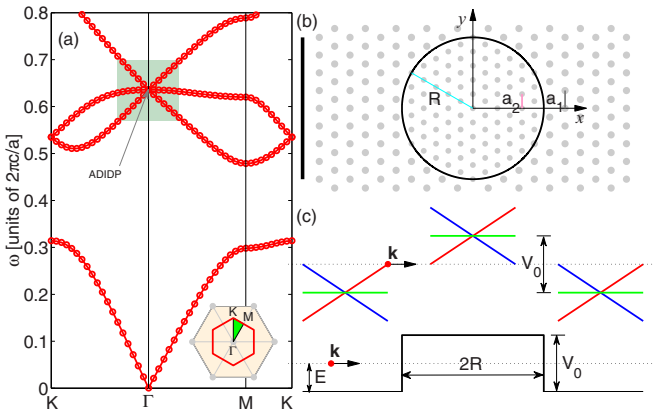

FIG. 1. Pseudospin-1 band structure and the underlying photonic lattice structure. The lattice has a triangular configuration constructed by cylindrical alumina rods in air. (a) The band structure with an accidental-degeneracy-induced Dirac point at the center of the first Brillouin zone, (b) sketch of the physical lattice, and (c) band structures outside and inside of the scatterer. A possible experimental parameter setting is $a_1 = 17$ mm, $r_1 = 0.203a_1$, $a_2 = 0.8a_1$, and $r_2 = 0.203a_2$. The dielectric constant of the alumina rod is 8.8.

section $\Sigma_{\rm tr}$ to characterize the scattering dynamics. (It should be noted that the total cross section Σ is another usual quantity for characterizing superscattering with results consistent with those for the transport cross section; see Appendix B for details.) The transport cross section is defined in terms of the scattering coefficients A_l as

$$\Sigma_{\rm tr}/R = (4/x)\sum_{l=-\infty}^{\infty}\{|A_l|^2 - {\rm Re}[A_l(A_{l+1})^*]\}, \qquad (1)$$

where A_l can be obtained through the standard method of partial-wave decomposition [1]. For convenience, we define $\rho \equiv V_0 R$ and $x \equiv kR$. At low energies, i.e., $x \ll 1$, scattering is dominated by the lowest angular momentum channels $l = 0, \pm 1$. To reveal the relativistic quantum nature of the scattering process, we focus on the under-barrier scattering regime, i.e., $x < \rho$, so that manifestations of phenomena such as Klein tunneling are pronounced. We define two subregimes of low-energy scattering: $1 < \rho$ and $x < \rho < 1$, where the former corresponds to the case of a scatterer with a large scattering potential. The weak-scatterer subregime, i.e., $x < \rho < 1$, is one in which the counterintuitive phenomenon of superscattering arises. Specifically, for $x < \rho < 1$, we obtain the leading coefficients as

$$A_0 \approx -P_0/(P_0 + iQ_0),$$
$$A_{\pm 1} \approx -P_1/[P_1 + i(4 + Q_1)], \qquad (2)$$

where $P_0 = \pi x$ and

$$Q_0 = 2\{x\ln(\gamma_E x/2) - J_0(\rho - x)/[J_1(\rho - x)]\},$$

with $\ln\gamma_E \approx 0.577\cdots$ being Euler's constant and P_1, Q_1 given by relations $[P_1, Q_1] = x[P_0, Q_0]$. Using these relations, we obtain

$$\frac{\Sigma_{\rm tr}}{R} = \frac{4P_0^2}{x(P_0^2 + Q_0^2)}\left\{1 - \frac{8Q_1}{P_1^2 + (4 + Q_1)^2}\right\}. \qquad (3)$$

We first show that, in our scattering system, all the conventional resonances will disappear in the weak-scatterer regime ($\rho < 1$). To make an argument, we examine the case of a scatterer with large scattering potential: $\rho > 1$, where the transport cross section as a function of x and ρ is given by (see Appendix A for a detailed derivation)

$$\frac{\Sigma_{\rm tr}}{R} \approx \frac{4}{x}\left(\frac{(\pi x)^2}{(\pi x)^2 + 4[\rho - \rho_{0,m} + x\ln(\gamma_E x/2)]^2}\right) + \frac{8}{x}\left(\frac{(\pi x^3)^2}{(\pi x^3)^2 + 4(\rho - \rho_{1,n} - x)^2}\right), \qquad (4)$$

with $m,n = 1,2,3,\ldots$ and $\rho_{0,m},\rho_{1,n}$ denoting the mth and nth zeros of the Bessel functions J_0 and J_1, respectively. The resonances occur about $\rho \approx \rho_{0,m},\rho_{1,n}$ for $x \ll 1$ and thus are well separated with a minimum position at $\rho \approx 2.4$. This indicates that the locations of such resonances satisfy $\rho > 2$, which is not possible in the small-scattering-potential regime $\rho < 1$. In conventional scattering systems where the Born approximation applies, no additional resonances will emerge in the small-scattering-potential regime $\rho < 1$.

For sufficiently weak scatterer strength ($\rho \ll 1$), the prefactor in (3), i.e.,

$$4P_0^2/[x(P_0^2 + Q_0^2)] \approx \pi^2 J_1^2(\rho - x)x/[J_0^2(\rho - x)] \to (\pi^2/4)(\rho - x)^2 x \ll 1,$$

is off resonance. The remaining factor characterizes the emergence of a type of (unconventional) revival resonance at $Q_1 + 4 = 0$, which is unexpected because the scatterers are sufficiently weak that, according to the conventional Born theory, no scattering resonances are possible. The resonant condition can be obtained explicitly from the constraint

$$Q_1 + 4 = 0 \Rightarrow xJ_0(\rho - x) = 2J_1(\rho - x).$$

We obtain $\rho = 2x$ for $\rho \ll 1$. The surprising feature of a revival resonance is that it persists no matter how weak the scatterer is. As a result, superscattering can occur for arbitrarily weak scatterer strength. One example is shown in Fig. 2(a), where a good agreement between the theoretical prediction and numerical simulation is obtained. For comparison, results for the corresponding pseudospin-1/2 wave scattering system governed by the conventional massless Dirac equation are shown in Fig. 2(b), where scattering essentially diminishes for near-zero scatterer strength, indicating complete absence of superscattering.

To characterize superscattering in a more quantitative manner, we obtain from Eq. (3) the associated resonance width as $\Gamma \sim \pi\rho^3/8$ and the closed approximation form as

$$\frac{\Sigma_{\rm tr}}{R} \approx \frac{\pi^2}{4}\rho^2 x\left[1 + \frac{16x\rho}{\pi^2 x^4\rho^2 + 16(\rho - 2x)^2}\right]. \qquad (5)$$

In addition, at the resonance, we have

$$\left(\frac{\Sigma_{\rm tr}}{R}\right)_{\rm max} \approx \frac{\pi^2 x J_1^2(x)}{J_0^2(x)}\frac{32}{\pi^2 x^4}\bigg|_{x=\rho/2} \simeq \frac{16}{\rho}. \qquad (6)$$

A striking and counterintuitive consequence of (6) is that the weaker the scatterer $\rho \downarrow$ is, the larger the resulting maximum cross section $(\Sigma_{\rm tr}/R)_{\rm max} \uparrow$ is. This can be explained by noting that, due to the revival resonant scattering, an arbitrarily large

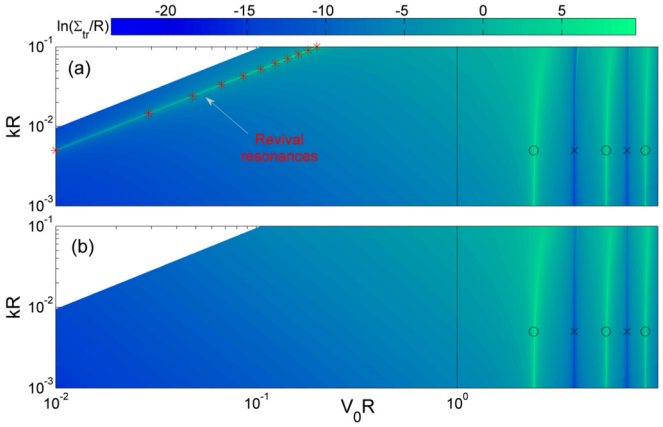

FIG. 2. Persistent revival resonances of pseudospin-1 particles from a weak circular scatterer at low energies. (a) Contour map of transport cross section in units of R (on a logarithmic scale) versus the scatterer strength $\rho = V_0 R$ and size $x = kR$ for relativistic quantum scattering of 2D massless pseudospin-1 particles. Revival resonances occur, which can lead to superscattering (see Fig. 3). (b) Similar plot for pseudospin-1/2 particles for comparison, where no resonances occur, implying total absence of superscattering. The scatterer is modeled as a circular steplike potential $V(r) = V_0\Theta(R - r)$, representing a finite-size scalar impurity or an engineered scalar type of scatterer. The markers correspond to the theoretical prediction, where the black circles and crosses are from $\rho \approx \rho_{0,m}, \rho_{1,n}$ (for $x \ll 1$), and the red stars follow the revival resonant condition given by $\rho = 2x$ for $\rho \ll 1$.

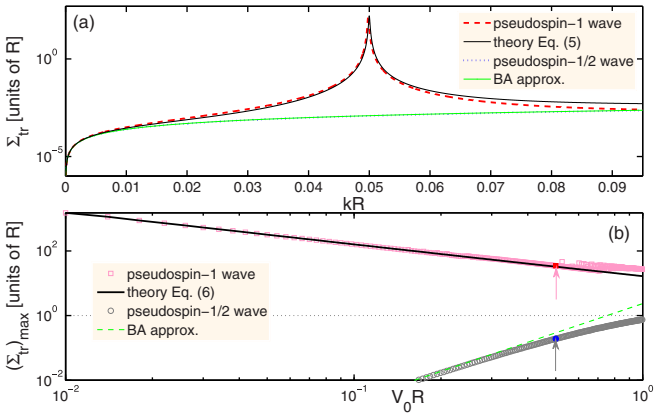

FIG. 3. Superscattering of pseudospin-1 wave. (a) Transport cross section as a function of $x \equiv kR$ for a weak scatterer of strength $\rho \equiv V_0 R = 0.1$ and (b) dependence of the maximum transport cross section on $V_0 R$.

cross section can be achieved for a sufficiently weak scatterer with its radius R much smaller than the incident wavelength $2\pi/k$ (i.e., in the deep-subwavelength regime $kR \ll 1$). In contrast, for a system hosting a pseudospin-1/2 wave under the same condition of $x < \rho \ll 1$ where the Born approximation applies [2], the maximum transport cross section is given by

$$\left(\frac{\Sigma_{\rm tr}}{R}\right)^{BA}_{\rm max} \approx \frac{\pi^2}{4}\rho^3. \tag{7}$$

Compared with that of pseudospin-1/2 particles, the scattering behavior revealed by Eq. (6) for pseudospin-1 particles is extraordinary and represents a phenomenon which, to our knowledge, has not been reported for any wave (especially matter wave) systems. The analytic predictions [Eqs. (6) and (7)] have been validated numerically, as shown in Fig. 3.

Further insights into superscattering can be obtained by examining the underlying wave-function patterns, as shown in Fig. 4. In particular, Figs. 4(a) and 4(c) and 4(b) and 4(d) show the distributions of the real part of one component of the spinor wave function $\mathrm{Re}(\Psi_2)$ for pseudospin-1/2 and pseudospin-1 particles, respectively, where the parameters are $V_0 R = 0.5$ and $kR = 0.2485$. The patterns in Figs. 4(b) and 4(d) correspond to the revival resonance indicated by the pink arrow in Fig. 3(b). We see that, even for such a weak scatterer, the incident pseudospin-1 wave of a much larger wavelength $\lambda = 2\pi/k \sim 25R$ is effectively blocked via trapping around the scatterer boundary, resulting in strong scattering. In contrast, for the conventional pseudospin-1/2 wave system, the weak scatterer results in only weak scattering, as shown in Figs. 4(a) and 4(c), which is anticipated from the Born theory.

III. EXPERIMENTAL TEST WITH PHOTONIC SYSTEMS

It is possible to test superscattering in experimental optical systems. Recent realization of photonic Lieb lattices consisting of evanescently coupled optical waveguides implemented by a femtosecond laser-writing technique [7–10] makes them suitable for studying the physics of pseudospin-1 Dirac cones. For example, in the tight-binding framework, for a homogeneous identical waveguide array with the same propagation constant

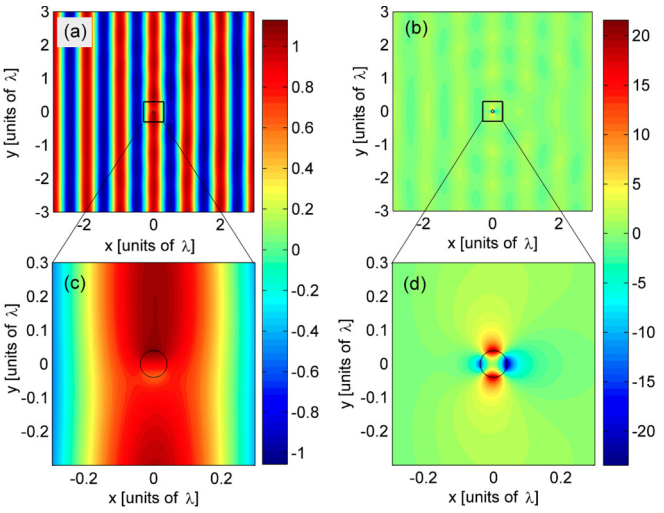

FIG. 4. Wave-function patterns associated with superscattering. For $V_0 R = 0.5$ and $kR = 0.2485$, the distribution of the real part of one component of the spinor wave function $\mathrm{Re}(\Psi_2)$ for (a) pseudospin-1/2 and (b) pseudospin-1 waves. (c) and (d) Magnification of part of (a) and (b), respectively. Both axes in (a)–(d) are in units of the incident wavelength λ. The color code denotes the quantity $\mathrm{Re}(\Psi_2)$.

β_0, the Hamiltonian in the momentum space is given by

$$\mathcal{H}_{TB}(\boldsymbol{k}) = \begin{pmatrix} \beta_0 & 2\kappa_x \cos(\frac{k_x}{2}) & 0 \\ 2\kappa_x \cos(\frac{k_x}{2}) & \beta_0 & 2\kappa_y \cos(\frac{k_y}{2}) \\ 0 & 2\kappa_y \cos(\frac{k_y}{2}) & \beta_0 \end{pmatrix}. \quad (8)$$

In the low-energy regime (measured from the β_0), the Hamiltonian is reduced to a generalized Dirac-Weyl Hamiltonian for spin-1 particles with β_0 analogous to the constant electronic gate (voltage) potential. As such, the superscattering phenomenon uncovered in our work can, in principle, be tested experimentally in photonic Lieb lattice systems through a particular design of the refractive index profile across the lattice to realize the scattering configuration.

Loading ultracold atoms into an optical Lieb lattice fabricated by interfering counterpropagating laser beams [11] provides another versatile platform to test our findings, where appropriate holographic masks can be used to implement the desired scattering potential barrier [18,19]. Synthetic photonic-crystal-based 2D pseudospin-1 wave systems are also promising for feasible experimental validation. For example, it was demonstrated experimentally [4–6] and theoretically [17,20] that a pseudospin-1 wave system can be realized in 2D dielectric photonic crystals via the principle of accidental degeneracy. Implementation of the scalar type of potential can be achieved by manipulating the length scale of the photonic crystals. From recent work on an "on-chip zero-index metamaterial" design [6] based on such a system, we note that the phenomenon of superscattering uncovered in this paper could be relevant to on-chip superscatterer fabrication, which is not possible for conventional wave systems.

IV. CONCLUSION AND DISCUSSION

In conclusion, we uncover a superscattering phenomenon in a class of 2D wave systems that host massless pseudospin-1 particles described by the Dirac-Weyl equation, where extraordinarily strong scattering (characterized by an unusually large cross section) occurs for an arbitrarily weak scatterer in the low-energy regime. Physically, superscattering can be attributed to the emergence of persistent revival resonances for scatterers of weak strength, to which the cross section is inversely proportional. These unusual features defy the prediction of the Born theory that is applicable to conventional electronic or optical scattering systems. Superscattering of pseudospin-1 waves thus represents a unconventional scattering scenario, and it is possible to conduct experimental tests using synthetic photonic systems.

An important issue is whether the superscattering uncovered in this paper is due to the presence of a flat band that implies an infinite density of states. Our answer is negative for the following reasons. Note that, measured from the three-band intersection point, the energy for the (dispersionless) flat-band states is zero outside and V_0 inside the scatterer, but for the two dispersion Dirac bands the energy is finite outside the scatterer and not equal to V_0 inside. For the elastic scattering considered in our work, the incident energy outside the scatterer is finite and less than V_0 as well. As a result, only the states belonging to the conical dispersion bands are available both inside and outside the scatterer and therefore are responsible for the superscattering phenomenon. Indeed, as demonstrated, superscattering is due to revival resonant scattering for states belonging to the conical dispersion bands that persist in the regime of arbitrarily weak scatterer strength. From another angle, if superscattering were due to the flat band, the phenomenon would arise in the conventional resonant scattering regime $V_0 R > 1$, which has never been observed.

While the flat band itself is not directly relevant to the superscattering behavior, its presence makes the structure of the relevant states belonging to the conical bands different from those, e.g., in a two-band Dirac cone system, giving rise to boundary conditions that permit discontinuities in the corresponding intensity distribution and tangent current at the interface. Interestingly, surface plasmon modes [see Fig. 4(d)] are excited at the interface when revival resonant scattering occurs, which is strongly localized and can be excited for an arbitrarily weak scatterer strength, leading to superscattering in the deep-subwavelength regime. These modes are created from the particular spinor structure of the photon states, which can be implemented by engineering light propagation in periodically modulated and/or arranged conventional dielectric materials (e.g., alumina) rather than within the material itself. Our finding of the superscattering phenomenon is thus striking and represents a scattering capability that goes beyond the Rayleigh-Gans limit or, equivalently, one defined by the Born approximation.

With respect to potential applications of the findings of this paper, it is worth emphasizing that the phenomenon of superscattering represents a way of controlling light behaviors beyond those associated with the conventional scattering scenario because, in our system [e.g., Fig. 1(b)], light is structured into three-component spinor states and behaves as a relativistic spin-1 wave in the underlying photonic lattice. There have been extensive recent experimental works demonstrating that such lattice systems can actually be realized. Our theoretical prediction is based on a general setting that effectively characterizes the low-energy physics underlying the photonic lattices.

ACKNOWLEDGMENTS

The authors would like to acknowledge support from the Vannevar Bush Faculty Fellowship program sponsored by the Basic Research Office of the Assistant Secretary of Defense for Research and Engineering and funded by the Office of Naval Research through Grant No. N00014-16-1-2828. This work was also supported by AFOSR under Grant No. FA9550-15-1-0151.

APPENDIX A: SCATTERING FORMALISM OF 2D MASSLESS SPIN-1 PARTICLES

1. Model Hamiltonian

As indicated in the main text, we consider the following perturbed Hamiltonian:

$$\mathcal{H} = H_0 + V(\boldsymbol{r}), \quad (A1)$$

where $V(\boldsymbol{r}) = V_0\Theta(R - r)$, with V_0 being the potential height.

Generally, far away from the scattering center (i.e., $r \gg R$), for an incoming flux along the x direction, the spinor wave function with the band index s takes the asymptotic form

$$|\Psi_s^{\gg}(\boldsymbol{r})\rangle = e^{ikx}|\boldsymbol{k}_0,s\rangle + \frac{f(\theta)}{\sqrt{-ir}}e^{ikr}|\boldsymbol{k}_\theta,s\rangle, \tag{A2}$$

where the vector $|\boldsymbol{k},s\rangle$ is the spinor plane-wave amplitude with wave vectors $\boldsymbol{k}_0 = (k,0)$ and $\boldsymbol{k}_\theta = k(\cos\theta, \sin\theta)$ defining the directions of the incident and scattering, respectively.

In our case, for the conical dispersion bands $s = \pm$, we obtain

$$|\boldsymbol{k},s\rangle = \frac{1}{2}\begin{pmatrix} e^{-i\theta} \\ \sqrt{2}s \\ e^{i\theta} \end{pmatrix}. \tag{A3}$$

With the definition of the current operator $\hat{\boldsymbol{J}} = (1/\hbar)\nabla_{\boldsymbol{k}} H(\boldsymbol{k}) = v_F(S_x, S_y)$, we have the scattered current

$$J_{\rm sc} = \frac{1}{r}\langle \boldsymbol{k}_\theta,s|f^*\hat{\boldsymbol{J}}\cdot\frac{\boldsymbol{k}_\theta}{k}f|\boldsymbol{k}_\theta,s\rangle = \frac{v_F}{r}|f(\theta)|^2, \tag{A4}$$

while the incident current $J_{\rm in} = \langle \boldsymbol{k}_0,s|\hat{\boldsymbol{J}}\cdot\boldsymbol{k}_0/k|\boldsymbol{k}_0,s\rangle = v_F$. The differential cross section is thus defined in terms of the scattering amplitudes $f(\theta)$ as

$$\frac{d\Sigma}{d\theta} = \frac{rJ_{\rm sc}}{J_{\rm in}} = |f(\theta)|^2. \tag{A5}$$

The other relevant cross sections can be calculated by definition; that is, the total cross section (TCS)

$$\Sigma = \int_0^{2\pi} d\theta \frac{d\Sigma}{d\theta}, \tag{A6}$$

and the transport cross section (TrCS)

$$\Sigma_{\rm tr} = \int_0^{2\pi} d\theta(1-\cos\theta)|f(\theta)|^2. \tag{A7}$$

In order to figure out the exact expression of $f(\theta)$, we expand the wave functions inside and outside the scatterer as a superposition of partial waves; that is, for $r > R$ (outside the scatterer),

$$|\Psi_s^{>}(\boldsymbol{r})\rangle = \sum_l \psi_{l,s}^{>}(\boldsymbol{r}), \tag{A8a}$$

and for $r < R$ (inside the scatterer),

$$|\Psi_s^{<}(\boldsymbol{r})\rangle = \sum_l \psi_{l,s}^{<}(\boldsymbol{r}), \tag{A8b}$$

where $\psi_{l,s}^{>}$ and $\psi_{l,s}^{<}$ are the partial waves defined in terms of the cylindrical wave eigenfunctions of the reduced Hamiltonian $\mathcal{H}$ that reads, in polar coordinates $\boldsymbol{r} = (r,\theta)$,

$$\mathcal{H} = \frac{\hbar v_F}{\sqrt{2}}\begin{pmatrix} 0 & \hat{L}_- & 0 \\ \hat{L}_+ & 0 & \hat{L}_- \\ 0 & \hat{L}_+ & 0 \end{pmatrix} + V(r), \tag{A9}$$

with the compact operator

$$\hat{L} = -ie^{i\tau\theta}\left(\partial_r + i\frac{\partial_\theta}{r}\right)$$

and $V(r) = V_0\Theta(R-r)$ being the circular symmetric scalar-type scattering potential. It is evident that $[\mathcal{H},\hat{\mathcal{J}}_z] = 0$, with the definition of $\hat{\mathcal{J}}_z = -i\hbar\partial_\theta + \hbar S_z$. As such, $\mathcal{H}$ acting on the spinor eigenfunctions of $\hat{\mathcal{J}}_z$ yields

$$\mathcal{H}\varphi_{l,s} = E\varphi_{l,s}, \tag{A10}$$

where the wave functions φ_l simultaneously satisfy $\hat{\mathcal{J}}_z\varphi_l = \hbar l\varphi_l$, with l being an integer. After some standard derivations, we obtain for the conical bands (i.e., $s = \pm$)

$$\varphi_{l,s}^{(0,1)}(\boldsymbol{r}) = \frac{1}{2\sqrt{\pi}}\begin{pmatrix} h_{l-1}^{(0,1)}(qr)e^{-i\theta} \\ i\sqrt{2}sh_l^{(0,1)}(qr) \\ -h_{l+1}^{(0,1)}(qr)e^{i\theta} \end{pmatrix}e^{il\theta}, \tag{A11}$$

where $q = |E-V|/\hbar v_F$ and $s = \mathrm{sgn}(E-V)$. The radial function $h_l^{(0)} = J_l$ is Bessel's function, and $h_l^{(1)} = H_l^{(1)}$ is Hankel's function of the first kind. The partial waves outside the scatterer ($r > R$) are therefore given by

$$\psi_{l,s}^{>}(\boldsymbol{r}) = \sqrt{\pi}i^{l-1}\left[\varphi_{l,s}^{(0)} + A_l\varphi_{l,s}^{(1)}\right], \tag{A12a}$$

while inside the scatterer ($r < R$) the partial waves read

$$\psi_{l,s}^{<}(\boldsymbol{r}) = \sqrt{\pi}i^{l-1}B_l\varphi_{l,s'}^{(0)}, \tag{A12b}$$

where A_l and B_l denote the elastic partial-wave reflection and transmission coefficients in the l angular channel, respectively. In order to obtain the explicit expressions of the partial-wave coefficients, relevant boundary conditions (BCs) are needed.

2. Boundary conditions

Recalling the commutation relations $[\hat{\mathcal{J}}_z,\mathcal{H}] = 0$, we generally define a spinor wave function in polar coordinates,

$$\psi(r,\theta) = [\psi_1,\psi_2,\psi_3]^T = \begin{pmatrix} \mathcal{R}_1(r)e^{-i\theta} \\ \mathcal{R}_2(r) \\ \mathcal{R}_3(r)e^{i\theta} \end{pmatrix}e^{il\theta}, \tag{A13}$$

which satisfies

$$\mathcal{H}\psi = E\psi. \tag{A14}$$

Substituting Eq. (A13) into the wave equation (A14) and eliminating the angular components finally yield the following (one-dimensional first-order ordinary differential) radial equation:

$$\frac{-i}{\sqrt{2}}\begin{pmatrix} 0 & \frac{d}{dr}+\frac{l}{r} & 0 \\ \frac{d}{dr}-\frac{l-1}{r} & 0 & \frac{d}{dr}+\frac{l+1}{r} \\ 0 & \frac{d}{dr}-\frac{l}{r} & 0 \end{pmatrix}\begin{pmatrix} \mathcal{R}_1(r) \\ \mathcal{R}_2(r) \\ \mathcal{R}_3(r) \end{pmatrix}$$

$$= \frac{E-V(r)}{\hbar v_F}\begin{pmatrix} \mathcal{R}_1(r) \\ \mathcal{R}_2(r) \\ \mathcal{R}_3(r) \end{pmatrix}. \tag{A15}$$

Directly integrating the radial equation above over a small interval $r \in [R-\eta, R+\eta]$ defined around an interface at $r = R$ and then taking the limit $\eta \to 0$, we obtain

$$\mathcal{R}_2(R-\eta) = \mathcal{R}_2(R+\eta),$$

$$\mathcal{R}_1(R-\eta) + \mathcal{R}_3(R-\eta) = \mathcal{R}_1(R+\eta) + \mathcal{R}_3(R+\eta), \tag{A16}$$

provided that the potential $V(r)$ and the radial function components $\mathcal{R}_{1,2,3}(r)$ are all finite. Reformulating such continuity conditions in terms of the corresponding wave function yields the BCs that we seek,

$$\psi_2^<(R,\theta)=\psi_2^>(R,\theta),$$

$$\psi_1^<(R,\theta)e^{i\theta}+\psi_3^<(R,\theta)e^{-i\theta}=\psi_1^>(R,\theta)e^{i\theta}+\psi_3^>(R,\theta)e^{-i\theta}. \tag{A17}$$

3. Far-field solutions: $r \gg R$

Using the asymptotic form of the Hankel function $H_l^{(1)}(kr)\sim\sqrt{2/\pi kr}e^{i(kr-l\pi/2-\pi/4)}$ and evaluating the outside wave function given in Eq. (A8a) at $r\gg R$, we arrive at

$$|\Psi_s^{\gg}(\boldsymbol{r})\rangle=e^{ikx}|\boldsymbol{k}_0,s\rangle+\frac{-i\sqrt{2/\pi k}\sum_l A_l e^{il\theta}}{\sqrt{-ir}}e^{ikr}|\boldsymbol{k}_\theta,s\rangle. \tag{A18}$$

It is evident from Eqs. (A18) and (A2) that

$$f(\theta)=-i\sqrt{\frac{2}{\pi k}}\sum_l A_l e^{il\theta}. \tag{A19}$$

Imposing relevant BCs given in Eq. (A17) on the total wave functions of both sides at the interface $r=R$, we have

$$B_l J_l(qR)=ss'\big[J_l(kR)+A_l H_l^{(1)}(kR)\big],$$

$$B_l X_l^{(0)}(qR)=X_l^{(0)}(kR)+A_l X_l^{(1)}(kR), \tag{A20}$$

where $X_l^{(0,1)}=h_{l-1}^{(0,1)}-h_{l+1}^{(0,1)}$. Solving the equation above, we finally determine the unknown coefficients

$$A_l=-\frac{J_l(qR)X_l^{(0)}(kR)-ss'X_l^{(0)}(qR)J_l(kR)}{J_l(qR)X_l^{(1)}(kR)-ss'X_l^{(0)}(qR)H_l^{(1)}(kR)} \tag{A21}$$

and

$$B_l=\frac{H_l^{(1)}(kR)X_l^{(0)}(kR)-X_l^{(1)}(kR)J_l(kR)}{H_l^{(1)}(kR)X_l^{(0)}(qR)-ss'X_l^{(1)}(kR)J_l(qR)}. \tag{A22}$$

Using the basic relations of $J_{-l}=(-)^l J_l$ and $H_{-l}^{(1)}=(-)^l H_l^{(1)}$, one can show the following symmetries:

$$A_{-l}=A_l,\quad B_{-l}=B_l. \tag{A23}$$

As such, the resulting probability density $\rho=\langle\Psi_s(\boldsymbol{r})|\Psi_s(\boldsymbol{r})\rangle$ and local current density $\boldsymbol{j}=\langle\Psi_s(\boldsymbol{r})|\hat{\boldsymbol{J}}|\Psi_s(\boldsymbol{r})\rangle$ can be calculated accordingly. In addition, the relevant scattering amplitudes $f(\theta)$ can be exactly obtained according to Eq. (A19) and hence related cross section given in Eqs. (A6) and (A7).

4. Derivation of Equation (4)

By definition, the transport cross section can be obtained as

$$\frac{\Sigma_{\rm tr}}{R}=\frac{4}{x}\sum_{l=-\infty}^{\infty}\{|A_l|^2-{\rm Re}[A_l(A_{l+1})^*]\}, \tag{A24}$$

with A_l being the reflection coefficients given in Eq. (A21). For $x\ll 1$, scattering is dominated by the lowest angular momentum channels $l=0,\pm 1$. As a result, the transport cross section can be approximated as

$$\frac{\Sigma_{\rm tr}}{R}\approx\frac{4}{x}\{|A_0|^2+2|A_1|^2-2{\rm Re}[A_0(A_1)^*]\}, \tag{A25}$$

where

$$A_0\approx-\frac{\pi x}{\pi x+i2[x\ln(\gamma_E x/2)-J_0(\rho)/J_1(\rho)]}$$

$$=-\frac{P_0}{P_0+iQ_0} \tag{A26a}$$

and

$$A_{\pm1}\approx-\frac{\pi x^3}{\pi x^3+i2[J_1(\rho)/J_1'(\rho)-x]}$$

$$=-\frac{P_2}{P_2+iQ_2}, \tag{A26b}$$

provided that the scattering potential is large, $\rho>1$.

Substituting Eqs. (A26a) and (A26b) into Eq. (A25), we obtain

$$\frac{\Sigma_{\rm tr}}{R}\approx\frac{4}{x}\left\{\frac{P_0^2}{P_0^2+Q_0^2}+2\frac{P_2^2}{P_2^2+Q_2^2}-2\frac{P_0P_2Q_0Q_2}{(P_0^2+Q_0^2)(P_2^2+Q_2^2)}\right\}. \tag{A27}$$

Since $P_2=x^2P_0=\pi x^3\ll 1$, the transport cross section will approach $\Sigma_{\rm tr}/R\sim 4/x(8/x)$ about $Q_0=0(Q_2=0)$, and $\Sigma_{\rm tr}/R\sim x\ll 1$ otherwise. It is thus reasonable to reduce Eq. (A27) to

$$\frac{\Sigma_{\rm tr}}{R}\approx\frac{4}{x}\left\{\frac{P_0^2}{P_0^2+Q_0^2}+2\frac{P_2^2}{P_2^2+Q_2^2}\right\}, \tag{A28}$$

where $Q_0=2[x\ln(\gamma_E x/2)-J_0(\rho)/J_1(\rho)]$ and $Q_2=2[J_1(\rho)/J_1'(\rho)-x]$. Since they are from different terms and each term has considerable values near $Q_0=0$ or $Q_2=0$, we can expand Q_0 and Q_2 about the zeros of $J_0(\rho)$ and $J_1(\rho)$, respectively, to get

$$Q_0\approx 2\left[\rho-\rho_{0,m}+x\ln\frac{\gamma_E x}{2}\right] \tag{A29a}$$

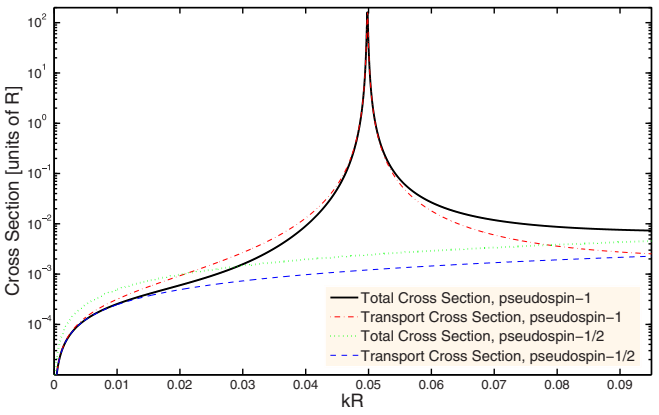

FIG. 5. Total and transport cross sections versus $x\equiv kR$ for a given weak-scattering potential $\rho\equiv V_0R=0.1$ in cases of pseudospin-1 and pseudospin-1/2.

and

$$Q_2 \approx 2(\rho - \rho_{1,n} - x), \tag{A29b}$$

with $m,n = 1,2,3,\ldots$ and $\rho_{0,m}$ and $\rho_{1,n}$ denoting the mth and nth zeros of the Bessel functions J_0 and J_1, respectively.

Substituting these into Eq. (A28), we arrive at Eq. (4) in the main text.

APPENDIX B: CHARACTERIZING SUPERSCATTERING WITH THE TOTAL CROSS SECTION

The total cross section Σ is an alternative quantity to characterize superscattering, with results consistent with those of the transport cross section, as shown in Fig. 5. In particular, from the total-cross-section curves (black and green), one can infer the same scattering behaviors as from the transport cross section. In fact, with the definition of total cross section $\Sigma/R = 4/x \sum_l |A_l|^2$, we can obtain a closed-form formula in the weak-scattering-potential regime:

$$\frac{\Sigma}{R} \approx \frac{\pi^2}{4}\rho^2 x\left[1 + \frac{8x^2}{\pi^2(\rho - x)^2x^4 + 16(\rho - 2x)^2}\right]. \tag{B1}$$

For $\rho = 2x$, the total cross section gives the same resonant peak value, $\sim 16/\rho$, as the transport cross section would.

[1] L. I. Schiff, *Quantum Mechanics*, 3rd ed. (McGraw-Hill, New York, 1968).

[2] J.-S. Wu and M. M. Fogler, Phys. Rev. B **90**, 235402 (2014).

[3] R. G. Newton, *Scattering Theory of Waves and Particles*, 2nd ed. (Springer, Berlin, 1982).

[4] X. Huang, Y. Lai, Z. H. Hang, H. Zheng, and C. T. Chan, Nat. Mater. **10**, 582 (2011).

[5] P. Moitra, Y. Yang, Z. Anderson, I. I. Kravchenko, D. P. Briggs, and J. Valentine, Nat. Photon. **7**, 791 (2013).

[6] Y. Li, S. Kita, P. Muñoz, O. Reshef, D. I. Vulis, M. Yin, M. Lončar, and E. Mazur, Nat. Photon. **9**, 738 (2015).

[7] D. Guzmán-Silva, C. Mejía-Cortés, M. A. Bandres, M. C. Rechtsman, S. Weimann, S. Nolte, M. Segev, A. Szameit, and R. A. Vicencio, New J. Phys. **16**, 063061 (2014).

[8] S. Mukherjee, A. Spracklen, D. Choudhury, N. Goldman, P. Öhberg, E. Andersson, and R. R. Thomson, Phys. Rev. Lett. **114**, 245504 (2015).

[9] R. A. Vicencio, C. Cantillano, L. Morales-Inostroza, B. Real, C. Mejía-Cortés, S. Weimann, A. Szameit, and M. I. Molina, Phys. Rev. Lett. **114**, 245503 (2015).

[10] F. Diebel, D. Leykam, S. Kroesen, C. Denz, and A. S. Desyatnikov, Phys. Rev. Lett. **116**, 183902 (2016).

[11] S. Taie, H. Ozawa, T. Ichinose, T. Nishio, S. Nakajima, and Y. Takahashi, Sci. Adv. **1**, e1500854 (2015).

[12] R. Shen, L. B. Shao, B. Wang, and D. Y. Xing, Phys. Rev. B **81**, 041410 (2010).

[13] D. Bercioux, D. F. Urban, H. Grabert, and W. Häusler, Phys. Rev. A **80**, 063603 (2009).

[14] D. Bercioux, N. Goldman, and D. F. Urban, Phys. Rev. A **83**, 023609 (2011).

[15] N. Goldman, D. F. Urban, and D. Bercioux, Phys. Rev. A **83**, 063601 (2011).

[16] D. F. Urban, D. Bercioux, M. Wimmer, and W. Häusler, Phys. Rev. B **84**, 115136 (2011).

[17] A. Fang, Z. Q. Zhang, S. G. Louie, and C. T. Chan, Phys. Rev. B **93**, 035422 (2016).

[18] W. S. Bakr, J. I. Gillen, A. Peng, S. Folling, and M. Greiner, Nature (London) **462**, 74 (2009).

[19] B. Dóra, J. Kailasvuori, and R. Moessner, Phys. Rev. B **84**, 195422 (2011).

[20] J. Mei, Y. Wu, C. T. Chan, and Z.-Q. Zhang, Phys. Rev. B **86**, 035141 (2012).